SCIENTIFIC REPORTS

OPEN

SUBJECT AREAS:
ELECTRONIC PROPERTIES AND MATERIALS
ELECTRICAL AND ELECTRONIC ENGINEERING

Received
10 June 2014

Accepted
15 July 2014

Published
4 August 2014

Correspondence and requests for materials should be addressed to Q.C. (qiangcheng@emfield.org) or T.J.C. (tjcui@seu.edu.cn)

Broadband and Broad-Angle Low-Scattering Metasurface Based on Hybrid Optimization Algorithm

Ke Wang, Jie Zhao, Qiang Cheng, Di Sha Dong & Tie Jun Cui

State Key Laboratory of Millimeter Waves, Department of Radio Engineering Southeast University, Nanjing 210096, P. R. China.

A broadband and broad-angle low-scattering metasurface is designed, fabricated, and characterized. Based on the optimization algorithm and far-field scattering pattern analysis, we propose a rapid and efficient method to design metasurfaces, which avoids the large amount of time-consuming electromagnetic simulations. Full-wave simulation and measurement results show that the proposed metasurface is insensitive to the polarization of incident waves, and presents good scattering-reduction properties for oblique incident waves.

Metamaterials are engineered materials with unusual constitutive parameters such as negative permittivity and permeability[1–4]. They are usually composed by periodic resonant or non-resonant units with the characteristic dimensions much smaller than the wavelength[5–7]. One important application of the metamaterials is to achieve electromagnetic invisibility or transparency, which can greatly reduce the radar cross section (RCS) of metallic or dielectric targets[8–11]. The approach of optical transformation provides an efficient way to bend the incident waves along the boundary of a region to be hidden without perturbing the exterior fields[12–14]. Therefore perfect invisibility can be achieved with no backward or forward RCS. However, the objects inside are completely isolated, which makes such devices hindered in practical applications. Another promising method is based on the scattering cancellation[15–19], where metasurface has been utilized to wrap the objects, and it can provide additional surface reactance in order to generate anti-phase scattered fields. But the bandwidth of the metasurface is usually very limited. The radar absorbing material can also be used for RCS reduction, which transforms electromagnetic energy into heat. But the change of the object temperature will inevitably increase the detection possibility by infrared detectors.

In this paper, we develop a low RCS metasurface using the windmill-shaped unit. The phase of each unit is chosen to be distributed randomly. The reflected waves from each part of the metasurface will experience destructive inference due to the random phase difference, leading to electromagnetic diffusion for the scattering waves. The design of the proposed metasurface seems to be the counterpart of the traditional reflectarray, which requires the reflected waves to be steered over a range of directions. In order to redistribute the scattering energy into all the directions, a large phase swing (i.e., the available phase shift of the composing unit) is usually required, while the magnitude of the normalized reflection efficient for the unit is kept to approach zero (dB) at the same time. Similar techniques for RCS conduction based on the objects' coating have been reported in Refs. [15–17], where both the perfect conductor and artificial magnetic conductor (AMC) have been used to create a chess-board-like structure. The reflected waves from the two units have 180.phase difference, hence the destructive interference between the two waves will dramatically reduce the scattering field level. The bandwidth of such coating is also restricted since it is usually hard to design broadband AMC structures. The mechanism of the proposed metasurface mainly depends on the random distribution of the reflection phases, which is totally different from the mechanisms mentioned above.

Results

Metasurface is a two-dimensional equivalent of three-dimension metamaterial (see Fig. 1), which could be used to control the reflection and transmission properties for the incident waves[20–22], and therefore achieve some interesting functionalities such as focusing and wave bending[23–25]. Usually a metasurface is composed by periodic or aperiodic elements, which are printed on the surface of a thin substrate.

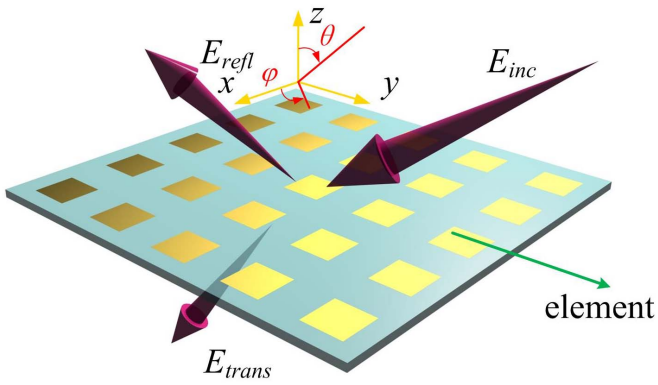

Figure 1 | Reflection and transmission of electromagnetic waves on the metasurface.

For a metasurface composed by large number of units with the same type and different geometrical dimensions, electromagnetic diffusions will be caused, resulting in low backward RCS[26]. However, it is usually hard to simulate the far-field scattering radiation pattern due to the burden of computation time and memory sources. Therefore the optimization of such metasurface for RCS reduction becomes very inefficient and impractical based on the simulation results. Actually the scattering pattern of such complex array can be rapidly synthesized when the mutual coupling between the adjacent elements are achieved through simple numerical simulations[27–28]. Let us consider a two dimensional metasurface composed by M*N units. When illuminated by a plane wave, the total scattering wave from the metasurface can be regarded as the superposition of the scattering wave from each basic element, which can be expressed as follows,

$$E_{total} = \sum_{m=1}^{M}\sum_{n=1}^{N} E_{m,n}(\theta,\varphi)\cdot e^{j\varphi_{m,n}} \tag{1}$$

where $E_{m,n}$ is the vectorial far-field scattered by the element [m,n]. θ and φ are the polar angle, and azimuthal angle, respectively. To obtain the scattering field of each element, the infinite periodic array model is adapted to calculate the coefficient $E_{m,n}$ in Eq. (1). We assume that every element is surrounded by the same cells when considering the influence of mutual coupling. This is an approximate model which does not correspond to the realistic metasurface configurations.

Here the induced surface currents from each element with periodic boundaries can be extracted from the numerical simulations. Take a small metasurface of 5*5 units for example, (as shown in Fig. 1(a)), the metallic windmill-shaped structure is selected as the basic element, and a perfect conductor layer is attached to the back of the substrate. From the equivalence principle, there are three kinds equivalent current on the surface of each element: the equivalent conducting current J_c on the conductor area and the equivalent electric current J_d and magnetic current M_d on the dielectric area[29–30]. In our simulation, the full-wave electromagnetic simulation tool FEKO is used to extract the equivalent currents mentioned above. When the metasurface is illuminated by a plane wave, the scattering field of each element can be written as

$$E^s(\mathrm{r}) = L_c[J_c] + L_d[J_d] + L_d[M_d] \tag{2}$$

where

$$\begin{aligned} L_c[J_c] &= -j\omega A_c - \nabla\phi_c \\ &= -\frac{j\omega\mu}{4\pi}\iint_{conductors} J_c(r')G(r:r')ds' - \frac{\nabla}{4\pi\varepsilon_0}\iint_{conductors}\rho_c(r')G(r:r')ds' \\ &= \frac{1}{j\omega 4\pi\varepsilon_0}\left[k_0^2\iint_{conductors} J_c(r')G(r:r')ds' + \nabla\iint_{conductors}\nabla'\cdot J_c(r')G(r:r')ds'\right] \end{aligned} \tag{3}$$

and

$$L_d[J_d] = -j\omega A_d - \nabla\phi_d \tag{4}$$

$$L_d[M_d] = -\frac{1}{\varepsilon_0}\nabla\times F \tag{5}$$

where

$$A = \frac{\mu}{4\pi}\iint_{dielectric} J_d(r')G(r:r')ds' \tag{6}$$

$$\phi = \frac{-1}{4\pi j\omega\varepsilon}\iint_{dielectric}\nabla'\cdot J_d(r')G(r:r')ds' \tag{7}$$

$$F = \frac{\varepsilon}{4\pi}\iint_{dielectric} M_d(r')G(r:r')ds' \tag{8}$$

and G(r : r') is the green function in free space.

Here the dimension of example is 60 mm × 60 mm, with several random-sized windmill-shaped structures. The radiation pattern the metasurface in Fig. 2(a) is also simulated by FEKO to check the agreement between the synthesis method and the numerical method, as shown by the black line and the red line in Fig. 2(b). It is clear that the synthesis method in Eq. (1) provides satisfactory prediction of the scattering pattern of the metasurface from the comparison. There are some discrepancies in the sidelobes from the two results in Fig. 2(b), which is mainly due to the mismatch of the boundary conditions used in the simulations. From the comparison between the simulated and synthesized radiation pattern, both results agree well which means that this model sufficiently provides a powerful means for radiation pattern prediction and optimization.

To get best performance of the metasurface, a particle swarm optimization (PSO) algorithm is utilized together with far-field pattern predition to achieve the optimal arrangement of the meta-atoms. In PSO algorithm every particle can be seen as an individual who searches for the optimum solution through cooperation in individuals and sharing information, which is an intelligent optimization algorithm proposed by Kenndey and Eberhart[31]. It has been widely applied to the optimization of various electromagnetic problems due to the merits like simple principle, few parameters and fast convergence. The potential solution can be deemed to a particle, whose mathematical description of the speed and location of next generation could be expressed as,

$$v_{ik}^{j+1} = \omega v_{ik}^{j} + c_1\times rand_1\times\left(pbest_{ik}^{j} - x_{ik}^{j}\right) + c_2\times rand_2\times\left(gbest_{k}^{j} - x_{ik}^{j}\right) \tag{9}$$

$$x_{ik}^{j+1} = x_{ik}^{j} + v_{ik}^{j+1} \tag{10}$$

Where ω is the inertia coefficient, c_1 and c_2 are the acceleration constants, which are used to adjust individual speed. $rand_1$ and $rand_2$ are random numbers between 0 and 1. $pbest_i^j$ is the individual optimal location, $gbest^j$ is the global optimal location. In the design of metasurface, x denotes the size of basic unit, and the performance of metasurface is evaluated by $fitness$(x), which is described as,

$$fitness = c_3\times\max(E_s) + c_4\times E_{s,1} \tag{11}$$

where c_3 and c_4 refer to weight coefficients. E_s denotes the total scattered field, $E_{s,1}$ denotes scattered field in the specific direction. Such fitness function aims at reducing the scattering energy mostly in the direction of maximum radiation.

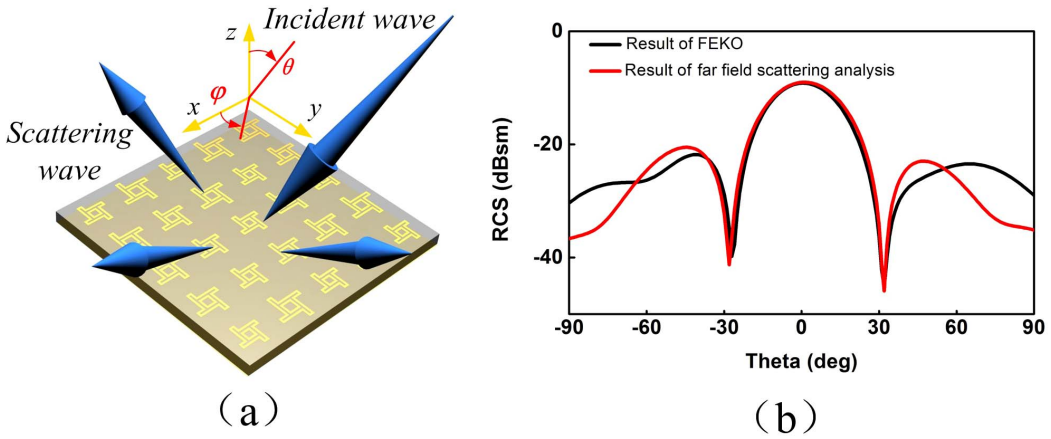

Figure 2 | (a) A metasurface containing 5*5 elements. (b) RCS of the metasurface in Figure 2(a) from the numerical simulation and far-field pattern analysis.

The design flow of the low RCS metasurface is shown in Fig. 3, where two modules have been used to get the desired optimal design. The PSO module evaluates the fitness, updates the particle speed and the population location (i.e. the meta-atom arrangements) in each iteration, and then sends the information to the far-field scattering pattern module. The latter gives the scattering pattern of the optimized metasurface based on the equivalent currents mentioned in last sections and calculates the reduction of RCS in the main scattering directions. Then the value of fitness is computed and returned to PSO module. After some iterations, we can get the optimal arrangement of metasurface with lowest RCS as required. The kernel of this flowchart is that the PSO module determines various combinations of basic unit, whose performances are judged by the far-field pattern analysis module to find the best solution.

A low RCS metasurface is designed, as shown in Fig. 4(a). The windmill shaped structure is selected to be the basic element. It is composed by an inner square ring and an outer irregular ring, and their resonance frequencies are designed to be very close in order to increase the operation bandwidth and the reflection phasing range. The curves of the reflection phase from 6 GHz to 14 GHz is almost linear, and they are nearly parallel with the change of L (the length of the branch of the outer ring), showing excellent broadband frequency response as required[32]. Here we choose the dimensions of the basic element in Fig. 4(a) as a=12 mm, g=0.4 mm, d=0.55 mm, h=4 mm. The substrate used in the simulation and experiment is F4B (ε_r=2.65+i.001) with the thickness 4 mm. The reflection phase of the basic element is extracted through the numerical simulations with the change of L at 8 GHz, 10 GHz, 12 GHz and 14 GHz (see

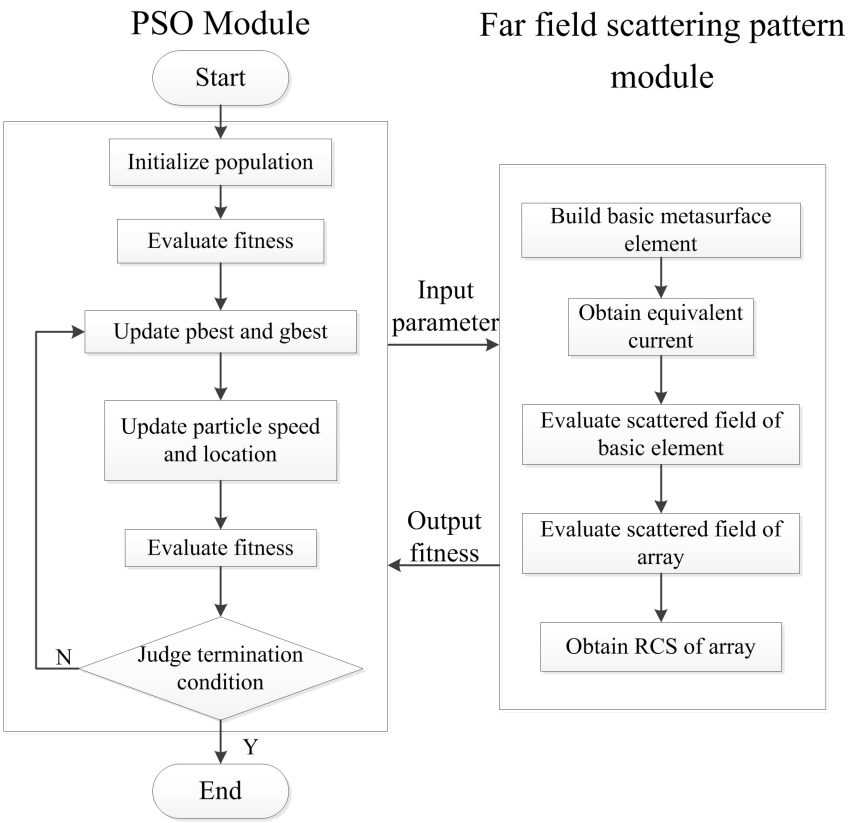

Figure 3 | **Flowchart for the design of low RCS metasurface.**

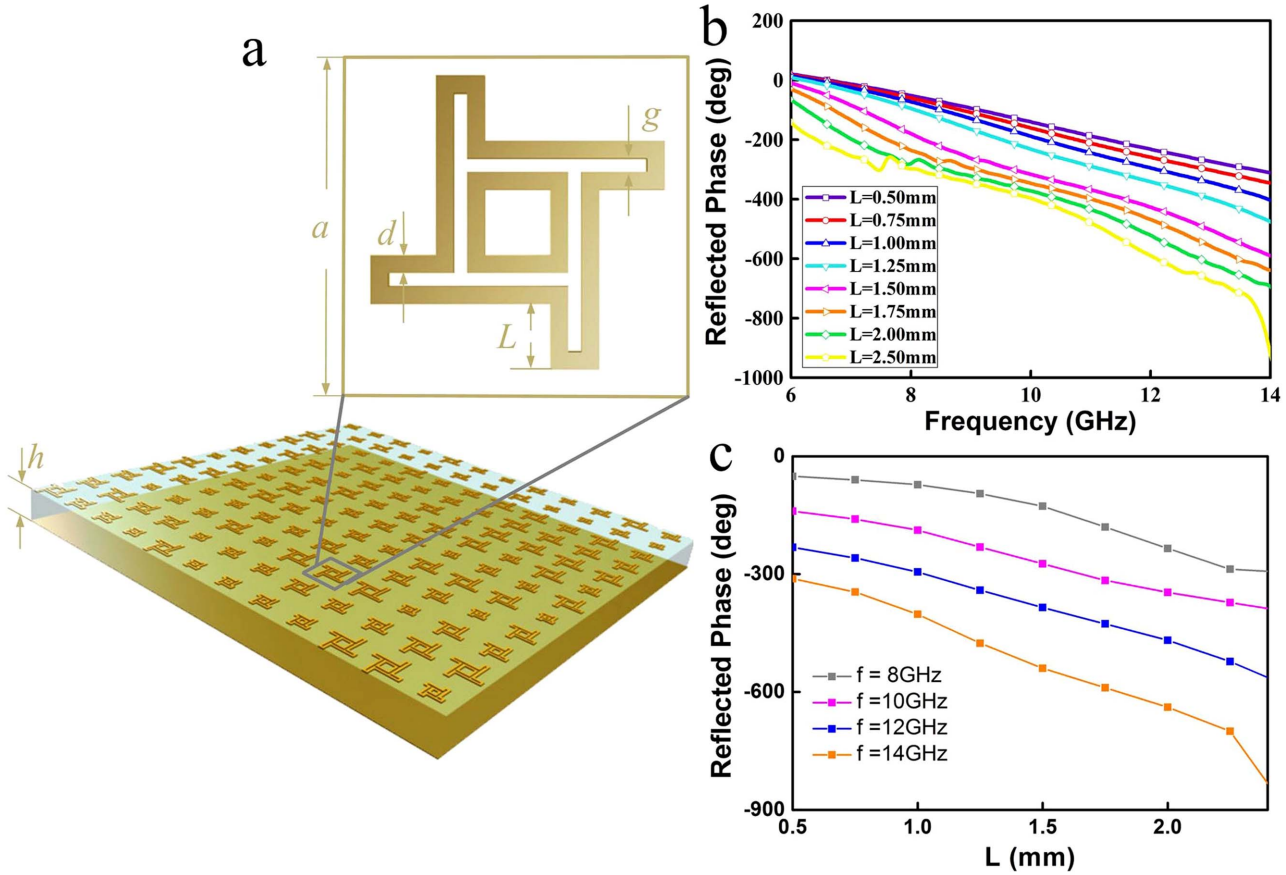

Figure 4 | (a) Basic element of the low RCS metasurface and the layout of the designed metasurface, (b) the reflection phase from 6 GHz to 14 GHz with the change of L in Fig. 4(a), (c) the reflection phase at different frequency with the change of L.

Fig. 4(c)). These curves are nearly parallel with each other, showing excellent linear frequency response, which is critical to guarantee the working bandwidth. It is clear that a large phasing range can be achieved when tuning the branch of the outer ring, which is important to ensure the performance of the low RCS metasurface.

In this design, for the simplicity of optimization, we choose elements with discrete phase distributions instead of continuous ones as mentioned above. Here eight windmill-shaped elements with different dimensions have been selected as the composing unit of the metasurface. When the length of the branch L is 0.6 mm, 0.825 mm, 1.05 mm, 1.26 mm, 1.47 mm, 1.75 mm, 2.05 mm and 2.38 mm respectively, the reflected phase is 45*n (n=1 to 8) degrees at the central frequency f =10 GHz, as illustrated in Fig. 4(b).

The whole metasurface is made up of 144 windmill-shaped units, and we need to find the optimal combination for the desired low RCS metasurface based on the eight basic elements. In our algorithm, a population size of 400 and a maximum of 100 iterations are predefined. It will take 9 hours to finish the every iteration based on the numerical simulation. However, the time spent in every iteration using the far-field scattering module is approximately 10 minutes

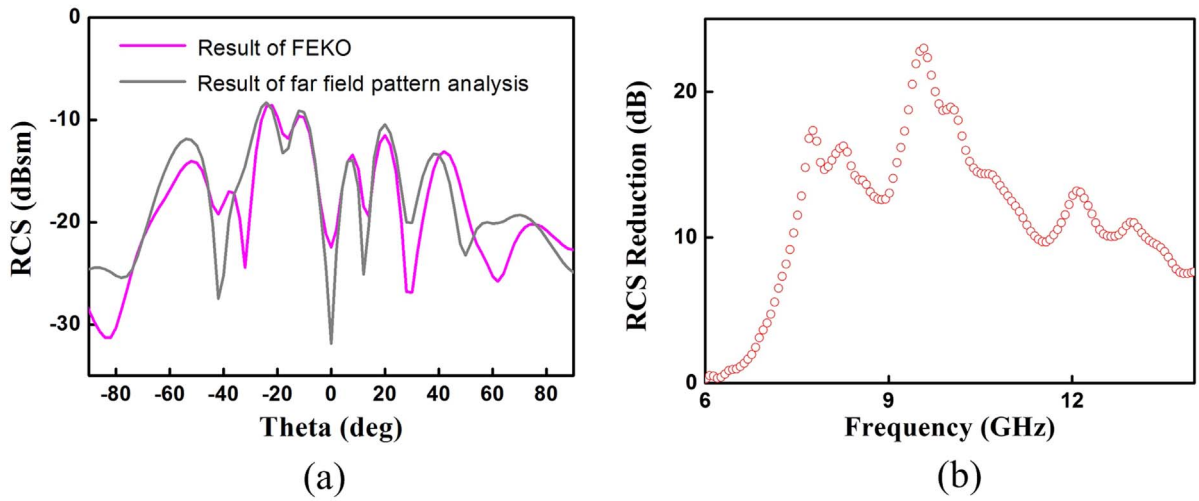

Figure 5 | (a) Far-field scattering pattern (φ = 0°) from numerical simulation (by FEKO) and far-field scattering pattern analysis, (b) simulated RCS reduction for normal incidence from 6 GHz to 14 GHz.

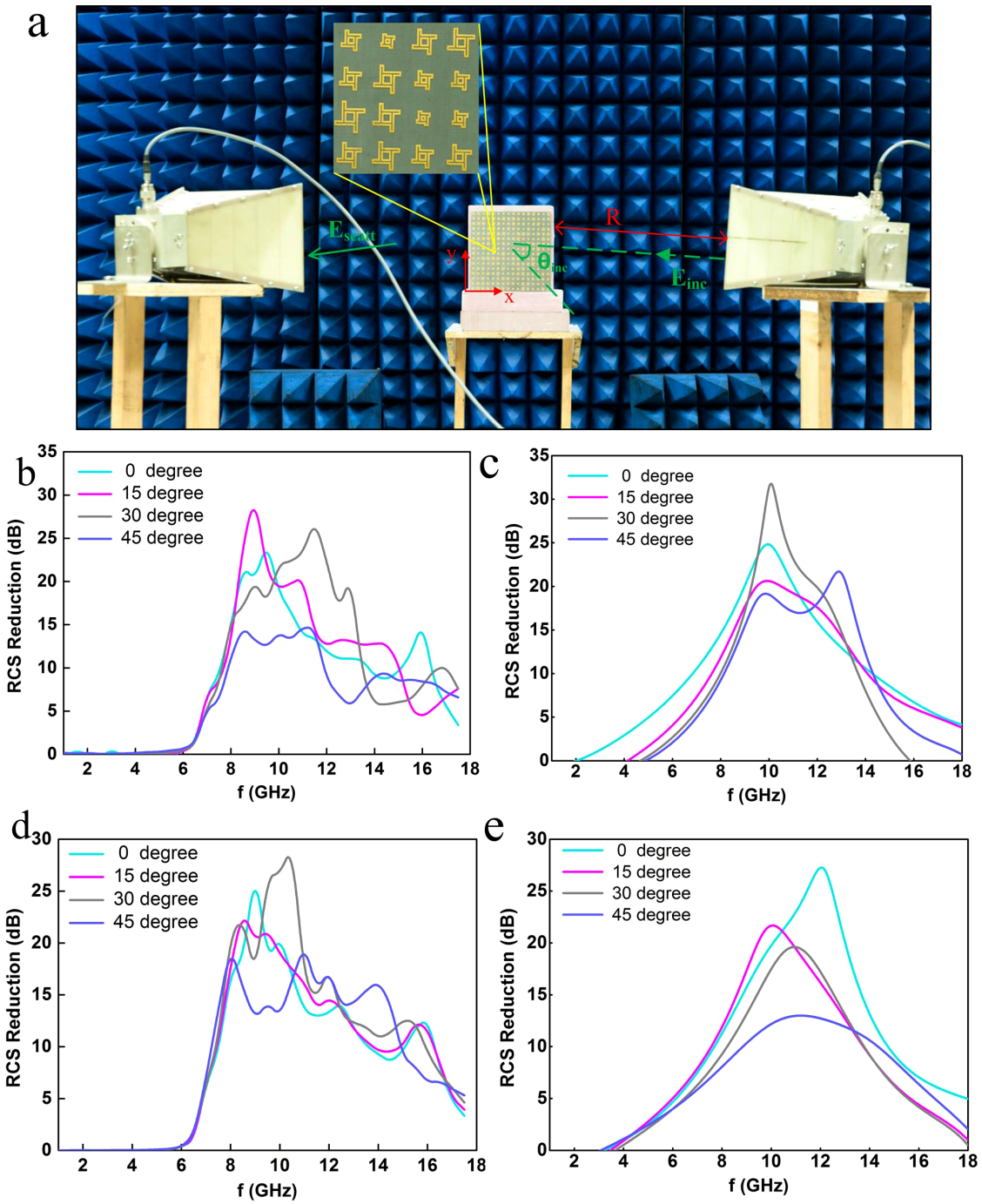

Figure 6 | (a) The experiment setup for RCS reduction, (b), (c) Simulated and experimental RCS reduction for various incident angles with vertical polarization. (d), (e) Simulated and experimental RCS reduction for various incident angles with horizontal polarization.

with the same hardware, which is much more efficient than before. After some iterations, the arrangement of the basic elements is finally determined with the layout shown in Fig. 4(a).

Fig. 5(a) shows the scattering pattern of the metasurface from full-wave simulations and far-field pattern prediction analysis. Both results seem to agree very well, which validates the whole design flow in Sec. 3. The RCS reduction for a bare metallic plate and the designed metasurface at different frequencies is illustrated in Fig. 5(b), where the RCS reduction is greater than 10 dB from 7 GHz to 13 GHz.

Discussion

In order to verify the theoretical analysis above, a larger metasurface containing 16 by 16 units, optimized by the algorithm, has been fabricated and tested, as depicted in Fig. 6. The transmitting and receiving horn antennas have been connected to a vector network analyzer (Agilent N5230C) to measure the RCS of the metasurface.

The simulated and measured RCS reductions for vertical and horizontal polarizations are shown in Figs. 6(c)(d) and Figs. 6(e)(f) respectively. The maximal RCS reduction can be found to exceed 30 dB as we can see from the measured results. The metasurface shows excellent broadband properties, where the RCS reduction is over 10 dB from 7 GHz to 14 GHz. With the increase of the incident angle, the bandwidth decreases a little due to the phase aberrations. Similarly, the maximum of RCS reduction is also decreased. However, low RCS properties are still kept for the proposed metasurface.

We have proposed the design algorithm for a low RCS metasurface with ultra-low backward scattering. The optimization method is used together with the far-field scattering pattern technique to find the desired broadband metasurface. The simulated and measured results demonstrate that the metasurface can effectively decrease the backward scattering from 7 GHz to 14 GHz, which is important for stealth applications in the future.

Methods

The sample is placed as high as the horn antennas in the experiment. The distance R (3 m) between antennas and sample is chosen far enough to avoid the near field effect. Pyramidal absorbing materials have been placed around the sample to decrease the unwanted reflections from the surroundings. In addition, a copper plate with the same size has also been measured for comparison. In the case of normal incidence, the transmitting and receiving horn antennas are placed adjacently, where the real incident angle is about 3 degree because of the restricted size of horn antennas. Both the transmitting and receiving horn antennas can move along the circumference trace to obtain RCS reductions at different scattering angle θ_{scatt}, where we only consider the case that the scattering angle θ_{scatt} equals to the incident angle θ_{inc}.

1. Koschny, T., Kafesaki, M., Economou, E. & Soukoulis, C. M. Effective medium theory of left-handed materials. *Phys. Rev. Lett.* **93**, 107402 (2004).
2. Simth, D. R., Padilla, W. J., Vier, D. C., Nemat-Nasser, S. C. & Schultz, S. Composite medium with simultaneously negative permeability and permittivity. *Phys. Rev. Lett.* **84**, 101103 (2000).
3. Shelby, R. A., Smith, D. R. & Schultz, S. Experimental verification of a negative index of refraction. *Science* **292**, 77–79 (2001).
4. Ziolkowski, R. W. & Heyman, E. Wave propagation in media having negative permittivity and permeability. *Phys. Rev. E* **64**, 056625 (2001).
5. Schurig, D., Mock, J. J. & Smith, D. R. Electric-field-coupled resonators for negative permittivity metamaterials. *Appl. Phys. Lett.* **88**, 041109 (2006).
6. Gay-Balmaz, P. & Martin, O. J. F. Electromagnetic resonances in individual and coupled split-ring resonators. *J. Appl. Phys.* **92**, 1497452 (2002).
7. Moser, H. O., Casse, B. D. F., Wilhelmi, O. & Saw, B. T. Terahertz response of a mircofabricated rod-split-ring-resonator electromagnetic metamaterial. *Phys. Rev. Lett.* **94**, 063901 (2005).
8. Schurig, D. *et al.* Metamaterial electromagnetic cloak at microwave frequencies. *Science* **314**, 977–980 (2006).
9. Liu, R. *et al.* Broadband ground-plane cloak. *Science* **323**, 366–369 (2009).
10. Ergin, T., Stenger, N., Brenner, P., Pendry, J. B. & Wegener, M. Three-dimensional invisibility cloak at optical wavelengths. *Science* **328**, 337–339 (2010).
11. Gömöry, F. *et al.* Experimental realization of a magnetic cloak. *Science* **335**, 1466–1468 (2012).
12. Jiang, W. X., Luo, C. Y., Mei, Z. L. & Cui, T. J. An ultrathin but nearly perfect direct current electric cloak. *Appl. Phys. Lett.* **102**, 014102 (2013).
13. Pendry, J. B., Schurig, D. & Smith, D. R. Controlling electromagnetic fields. *Science* **312**, 1780–1782 (2006).
14. Liu, X., Li, C., Yao, K., Meng, X. K. & Li, F. Invisibility cloaks modeled by anisotropic metamaterials based on inductor-capacitor networks. *IEEE Trans. Antennas Wireless Propag.* **8**, 1154–1157 (2009).
15. Paquay, M., Iriarte, J. C., Ederra, I., Gonzalo, R. & de Maagt, P. Thin AMC structure for radar cross-section reduction. *IEEE Trans. Antennas Propag.* **55**, 3630–3638 (2007).
16. de Cos, M. E., Alvarez, Y. & Las-Heras, F. A novel approach for RCS reduction using a combination of artificial magnetic conductors. *Prog. Electromagn. Res.* **107**, 147–159 (2010).
17. Treyakov, S. A. & Maslovsi, S. I. Thin absorbing structure for all incidence angles based on the use of a high-impedance surface. *Microw. Opt. Tech. Lett.* **38**, 175–178 (2003).
18. Yang, X. M., Zhou, X. Y., Cheng, Q., Ma, H. F. & Cui, T. J. Diffuse reflections by randomly gradient index metamaterials. *Opt. Lett.* **35**, 808–810 (2010).
19. Zhang, Y., Mittra, R. & Wang, B. Z. AMCs for ultra-thin and broadband RAM design. *Electron. Let.* **45**, 484–485 (2009).
20. Zhao, Y. & Alù, A. Manipulating Light Polarization with Ultrathin Plasmonic Metasurfaces. *Phys. Rev. B* **84**, 205428 (2011).
21. Kildishev, A. V., Boltasseva, A. & Shalaev, V. M. Planar Photonics with Metasurfaces. *Science* **339**, 6125 (2013).
22. Yu, N. & Capasso, F. Flat optics with designer metasurfaces. *Nat. Mater.* **13**, 139–150 (2014).
23. Gordon, J. A., Holloway, C. L. & Dienstfrey, A. A physical explanation of angle-independent reflection and transmission properties of metafilms/metasurfaces. *IEEE Trans. Antennas Wireless Propag.* **8**, 1127–1130 (2009).
24. Maci, S., Minatti, G., Casaletti, M. & Bosiljevac, M. Metasurfing: Addressing waves on impenetrable metasurfaces. *IEEE Trans. Antennas Wireless Propag.* **10**, 1499–1502 (2011).
25. Pfeiffer, C. & Grbic, A. Cascaded metasurfaces for complete phase and polarization control. *Appl. Phys. Lett.* **102**, 231116 (2013).
26. Chen, J., Cheng, Q., Zhao, J., Dong, D. S. & Cui, T. J. Reduction of Radar Cross Section Based on a Metasurface. *Prog. Electromagn. Res.* **146**, 71–76 (2014).
27. Encinar, J. A. Design of two-layer printed reflectarrays using patches of variable size. *IEEE Trans. Antennas Propag.* **49**, 1403–1410 (2001).
28. Li, H., Wang, B. Z., Guo, L., Shao, W. & Du, P. A far field pattern analysis technique for reflectarrays including mutual coupling between elements. *J. Electromagn. Waves Appl.* **23**, 87–95 (2009).
29. Sarkar, T. K. & Arvas, E. An integral equation approach to the analysis of finite microstrip antennas: volume/surface formulation. *IEEE Trans. Antennas Propag.* **38**, 3671659 (1990).
30. Sarkar, T. K., Rao, S. M. & Djordjevic, A. R. Electromagnetic scattering and radiation from finite microstrip structures. *IEEE Trans. microwave theory Tech.* **38**, 3803749 (1990).
31. Poli, R., Kennedy, J. & Blackwell, T. Particle swarm optimization. *Swarm intelligence* **1**, 33–57 (2007).
32. Li, H., Wang, B. Z. & Du, W. P. Novel Broadband Reflectarray Antenna with Windmill-Shaped Elements for Millimeter-Wave Application. *Int J Infrared Milli Waves* **28**, 339–344 (2007).

Acknowledgments

This work was supported by the National Science Foundation of China (60990320, 61138001, 61171026, and 60990324), National High Tech (863) Projects (2011AA010202 and 2012AA030402), 111 Project (111-2- 05) and the Natural Science Foundation of the Jiangsu Province BK2012019, and 20130202 Guangxi Experiment Center of Information Science, Guilin University of Electronic Technology.

Author contributions

Q.C. and T.J.C. conceived the idea. K.W. did the theoretical calculations and designed the samples. K.W., J.Z. and D.S.D. performed the measurements. K.W. and Q.C. wrote the manuscript based on input from all authors. All authors contributed to the discussions.

Additional information

Competing financial interests: The authors declare no competing financial interests.

How to cite this article: Wang, K., Zhao, J., Cheng, Q., Dong, D.S. & Cui, T.J. Broadband and Broad-Angle Low-Scattering Metasurface Based on Hybrid Optimization Algorithm. *Sci. Rep.* **4**, 5935; DOI:10.1038/srep05935 (2014).